A DYNAMIC PROGRAMMING SOLUTION TO TRACKING AND ELASTICALLY MATCHING LEFT VENTRICULAR WALLS IN CARDIAC CINE MRI

S.A. Tsaftaris[1]*, V. Andermatt*[1]*, A. Schlegel*[1]*, A.K. Katsaggelos*[1]*, D. Li*[2]*, R. Dharmakumar*[2]

[1]Dept. of Electrical Engineering
and Computer Science
Northwestern University, Evanston, IL 60208, USA
{stsaft, aggk}@eecs.northwestern.edu

[2]Dept. of Radiology
Northwestern University,
Chicago, IL 60611, USA
{d-li2, rohandkumar}@northwestern.edu

ABSTRACT

In this paper an algorithm to detect and elastically match the contours of the epicardial walls of the left ventricle (LV) in cardiac phase-resolved 2-D Magnetic Resonance (MR) images is presented. For both tasks, dynamic programming (DP) is used. A mask conforming to the six segment model of the LV is fitted on a reference image and propagated utilizing the elastic matching information. At its present form the algorithm requires minimal parameter corrections among different sets of cine MRI images. Future extensions include comparisons with contours hand labeled by imaging experts.

Index Terms— Magnetic resonance imaging, detection, Dynamic programming, registration, matching

1. INTRODUCTION

To determine insufficient blood circulation, the most common cause of heart attacks, short axis blood oxygen-dependent (BOLD) MR images of the LV are used. A six segment model is typically used to study the regional blood supply in the LV [1]. By examining the signal intensities of different LV sections in an MR image, it is possible to identify regional oxygen deficits, and the branch of the coronary artery that is affected [2]. Currently, each image is segmented by hand, a rather tedious and time consuming effort. Therefore, diagnosis has been generally based on a single image. Evaluating the full set of cardiac phase-resolved BOLD images for regional perfusion deficits, can increase the confidence of the diagnosis [3, 4].

There has been a great interest in computer-assisted myocardial contour delineation algorithms, since human effort can be reduced, and unbiased and consistent results can be produced [5]. Three major approaches exist: (i) active contour based methods where an initial contour is refitted near strong local image features by minimizing an energy function [6]; (ii) deformable parametric models with limited degrees of freedom [7, 8]; (iii) statistical description and learning based methods of local shape and brightness [9]; and combinations of the above [10, 11]. DP optimization has been used in medical imaging; for example in detecting, tracking and matching LV boundaries [12], and matching skeletonized angiographic images [13].

In this paper, a DP approach is presented to accurately detect the endocardial and epicardial boundaries of the LV, as well as, elastically match the epicardial boundaries, in polar coordinates. Section 2 discusses the detection of the LV boundaries, while section 3 presents the elastic matching of the epicardial boundaries. In section 4 test results are given, and finally, in section 5 conclusions and future extensions are offered.

2. CONTOUR DETECTION

Electrocardiogram (ECG)-gated, short axis cine (cardiac phase-resolved) magnetic resonance images are acquired within a single breath-hold ($\tilde{1}5$ second). Considering the application of the proposed system, the following realistic initializations are made from a user who: (i) initializes the algorithm by determining an ROI thus locating the LV in the MR image, (ii) selects the initial reference image (typically the end-systolic frame), (iii) selects an initial center of the LV blood chamber on the reference image, (iv) draws an initial epicardial contour on the reference image and (v) draws a line from the center of the LV chamber to the epicardial border. This line is used to generate the first 6 segment model mask. In the following, $c_t(s)$, is the point s of the contour c_t of image t in polar coordinates.

Due to the myocardium's circular shape in the short axis images, an example of which is shown in Fig. 1, the detection is performed in polar coordinates. The sought-after contour is located near image edges and has a linear shape (when the origin of the polar coordinate system is placed in the middle of the LV, as seen in Fig. 2).

2.1. Detecting the epicardial contour

The contour $r(\phi)$ is detected in polar coordinates by minimizing an energy cost function similar to [5, 14]. The total cost E_{tot} of the contour $r(\phi)$ is given by

$$E_{tot}(r(\phi)) = \sum_{\phi=1}^{N} (E_s(r(\phi),\phi) + E_t(r(\phi),\phi) + E_i(r(\phi),\phi) + E_p(r(\phi,\phi)),$$

where N is the total number of rays used to transform the image into polar coordinates. Subsequently each constraint is addressed.

Smoothness constraint:

$$E_s(R\{c_t(s-1)\}, R\{c_t(s)\}) = \omega_s \left(\frac{R\{c_t(s-1)\} - R\{c_t(s)\}}{f_{norm}} \right)^2$$

where ω_s is the weighting factor, and $R\{c_t(s-1)\}, R\{c_t(s)\}$ are the radii of the points $(s-1)$, and s on the contour. The normalization factor f_{norm} is necessary to accommodate various MRI spatial resolutions and is equal to 1% of the average radius $\bar{R}\{c_1\}$ of the hand-labeled contour.

Temporal constraint: This constraint allows for small temporal changes over the whole contour but penalizes large ones. The cost $E_t(R\{c_t(s-1)\}, R\{c_t(s)\})$ is 0, unless $|R\{c_{t-1}(s)\} - R\{c_t(s)\}| - \Delta R_{max} > 0$; then it is equal to $\omega_t \cdot (|R\{c_{t-1}(s)\} -$

$R\{c_t(s)\}| - \Delta R_{max})$. ω_t is a weighting factor; $|R\{c_{t-1}(s)\} - R\{c_t(s)\}|$ corresponds to the distance between the two contours at the same point; ΔR_{max} is the maximum change allowed and is used to limit the effect of small differences on the cost.

Image constraint: Due to the various tissue boundaries and interfaces there is variability in the desired edge location and the corresponding gradient value. The different edge profiles at the epicardial boundary can be seen clearly in Fig. 1. Different normalization factors are estimated on a the first image, and are utilized according to the sign of the edge operator's output. Assuming an initial hand-labeled contour, the following normalization factors are defined

$$f_{pos} = \text{ mean}(max(W(c_t(s)))),$$

for all s s.t. $|max(W(c_t(s)))| > |min(W(c_t(s))|$,

$$f_{neg} = \text{ mean}(\ min(W(c_t(s)))),$$

for all s otherwise. $W(\cdot)$ is a 1×5 search window centered at $c_t(s)$. Subsequently, the output of the 1-D gradient operator of [15] is normalized with the above factors according to its sign. The corresponding cost is

$$E_i(r, \phi) = -\omega_i \cdot |\Omega_{norm}(r, \phi)|\,,$$

where ω_i is the weight, and $\Omega_{norm}(r, \phi)$ is the normalized edge operator output.

Proximity constraint: To penalize cases where the algorithm is attracted by strong edges, (for example around the angle 75 in Fig. 2) the number of edges between the candidate contour and an internal "boundary" (see below) are used as a constraint,

$$E_p(r, \phi) = \omega_p \cdot \frac{1}{f_{norm}} \cdot \sum_{\widetilde{r}=r}^{R\{m_t(\phi)\}} M_{pt}(\widetilde{r}, \phi),$$

where $M_{pt}(\widetilde{r}, \phi)$ is 1 if $|\Omega_{norm}(\widetilde{r}, \phi)| > t_p$ and 0 otherwise (t_p is a user selected threshold), and $R\{m_t(\phi)\}$ is discussed below.

To distinguish between the epicardial and endocardial contours, the search area in each case is controlled. A DP algorithm is employed that finds a path through the polar image, creating an internal "boundary", which is smooth (as before) and not close to the edges (since the muscle texture is smooth), using the following constraints

$$E_{muscle}(s) = \omega_{em} \cdot |\Omega_{norm}(\vartheta\{c_t(s)\}, R\{c_t(s)\})| + \omega_{sm} \cdot \left(\frac{R\{c_t(s-1)\} - R\{c_t(s)\}}{f_{norm}} \right)^2,$$

where ω_{em}, ω_{sm} are the weights of the edge cost, and the smoothness constraint respectively, f_{norm} is the normalization factor described above, and $\vartheta\{c_t(s)\}$ corresponds to the angle of point s in the polar image.

2.2. DP implementation

For a point (r, ϕ_k) along a ray with angle ϕ_k, the cost is

$$E^0(r, \phi_k) = \min_{r_p \in [1,N]} \{E^0(r_p, \phi_{k-1}) + E_s(r_p, r)\} + E_i(r, \phi_k) + E_t(r, \phi_k) + E_p(r, \phi_k),$$

where N is the number of points in a ray. This propagation equation is used to find the cost of all points in a ray ($r = [1, N]$) for all rays ϕ_k, ($k = [3, M-1]$), with M the number of rays. Starting points for the first rays ($k = 1, 2$) are initially fixed. In the last ray ϕ_M, the cost for closing the contour $E_s(r, r_s)$ must be considered, i.e.,

$$E^0(r, \phi_M) = \min_{r_p \in [1,N]} \{E^0(r_p, \phi_p) + E_s(r_p, r)\} + E_i(r, \phi_M) + E_t(r, \phi_M) + E_p(r, \phi_M) + E_s(r, r_s).$$

This last equation is used to calculate the cost of all points in the last ray, where $r = [1, N]$. The best contour is obtained by backtracking the minimum cost point along the last ray.

To find the global optimal solution, the contour of all possible start points $r_s = [1, N], k = 1, 2$ must be determined. Finally, the starting point with the minimal total cost is chosen. To reduce computations, the user initializes the algorithm by selecting a start region that has a clearly visible contour with a single strong edge.

2.3. Detecting the endocardial contour

To detect the endocardial contour, a similar DP algorithm is employed. However, the temporal constraint is excluded due to its rapid movement. The cost function used is

$$E_i(r, \phi) = E_{iS}(r, \phi) + E_{iP}(r, \phi) + E_{iI}(r, \phi),$$

where the smoothness and physiological constraints are defined above, while $E_{iI}(r, \phi) = \omega_{iI}\,|\Omega_{norm}(r, \phi)|$. The advantage of this method is that the protruding papillary muscles can be excluded.

3. ELASTIC MATCHING

Oxygenation deficits in the LV appear as small regional intensity variations. It is therefore critical to elastically register subsequent images. The task of this section is to match contour points among two frames. The goal here is to propagate the 6-segment AHA model, therefore only the epicardial LV contours are matched. However, the same algorithm can be applied for the endocardial contours. Finally, the matched contours can be used as landmarks for spline based registration algorithms [3, 4].

c_t, c_{t+1}, and c_{t-1} denote the current, future, and previous contours respectively. Every point s of a contour $c_t(s)$ consists of an x- and y-components $(x_t(s), y_t(s))$ in the cartesian

In [12], the elementary constraints for matching two contours are given as:

- *Uniqueness constraint:* Every element of contour c_t has one match in the next contour c_{t+1}.
- *Monotonicity constraint:* No crossing displacement vectors are allowed. However, multiple points of contour c_t can point to the same point of c_{t+1}.
- *Gaps:* Unmatched regions on c_{t+1}, should be small.
- *Displacement smoothness:* The displacement vectors of consecutive points should vary smoothly.

The above constraints consider only shape related information; pixel values and temporal information are ignored. Furthermore, no provision is taken with respect to the extent of rotation. Therefore, the following constraints are introduced:

- *Smoothness between consecutive contours:* A temporal constraint is used to enforce smoothness of the displacement vectors of consecutive matchings.
- *Avoiding rotation:* To avoid rotation in the matching result, the length of the displacement vectors is considered.
- *Intensity:* Signal intensity differences in the polar image are included in the optimization.

3.1. Energy cost function

Expressed in mathematical form the energy cost for matching a point $c_t(s)$ to $c_{t+1}(k)$ is

$$\begin{aligned} E(c_t(s), c_{t+1}(k)) &= \frac{\omega_1}{\omega_{1N}} \cdot \left\| \vec{D}_t(s) - \vec{D}_t(s-1) \right\| \\ &+ \frac{\omega_2}{\omega_{5N}} \cdot \sum_{k=1}^{L_{t+1}} \sum_{p=1}^{L_{t+1}} M_t(s,k) \cdot M_t(s-1,p) \cdot (k-p-1)^2 \\ &+ \frac{\omega_3}{\omega_{3N}} \cdot \left\| \vec{D}_t(s) \right\| + \frac{\omega_4}{\omega_{4N}} \cdot \left\| \vec{D}_t(s) - \vec{v}_{pred}(s) \right\| \\ &+ \frac{\omega_2}{\omega_{2N}} \cdot \min_{r=-3..+3} \{ \, SAD(\, \Theta(\tilde{I}p_t, R\{c_t(s)\}, \vartheta\{c_t(s)\}) \\ &\qquad - \Theta(\tilde{I}p_{t+1}, R\{c_{t+1}(k)\} + r, \vartheta\{c_{t+1}(k)\}) \,) \, \}. \end{aligned} \tag{1}$$

The terms $\omega_1, \ldots, \omega_5$ and $\omega_{1N}, \ldots, \omega_{5N}$ denote the weights and the normalization factors for the displacement vector smoothness, gap, rotation, temporal, and intensity constraint, respectively. M_t and $\vec{D}_t(s)$ are the matching unit and displacement vector as in [12]. The normalization factors allow for the weights to be independent of the sizes of the contours, and the resolution of the MR images.

To find a prediction for the displacement vector $\vec{v}_{pred}(s)$ in the 4th term of Eq. 1, the displacement vectors of the previous matching $\vec{D}_{t-1}$ are utilized. However, since gaps are allowed there may be one, none, or many point(s) of c_{t-1} pointing to $c_t(s)$. Analytically, these three cases are:

Case 1: Exactly one point of c_{t-1} points to $c_t(s)$:

$$\vec{v}_{pred}(s) = \vec{v}_{prev}(s),$$

where $\vec{v}_{prev}(s)$ is the displacement vector from point c_{t-1} to $c_t(s)$.

Case 2: No point of the previous contour c_{t-1} points to $c_t(s)$. The predicted displacement of this point is computed by a weighted average of the neighboring displacements,

$$\vec{v}_{pred}(s) = \frac{\sum_{m=1}^{M} \frac{\vec{v}_{prev_m}(s)}{d_{prev}(s)} + \sum_{n=1}^{N} \frac{\vec{v}_{next_n}(s)}{d_{next}(s)}}{\frac{M}{d_{prev}(s)} + \frac{N}{d_{next}(s)}},$$

where M is the number of points on c_{t-1} which point to $c_t(j)$, for $j < s$. N is the number of points on c_{t-1} which point to $c_t(l)$ of $c_t(s)$, for $l > s$. d_{prev} and d_{next} are the distances defined as, $d_{prev} = s - j$ and $d_{next} = l - s$.

Case 3: Multiple points of c_{t-1} point to $c_t(s)$,

$$\vec{v}_{pred}(s) = \frac{\sum_{m=1}^{M} \vec{v}_{prev_m}(s)}{M},$$

where M is the number of points on c_{t-1} that point to $c_t(s)$.

In the last term of Eq.(1), SAD is the sum of all absolute element values of a given matrix. The function $\Theta(\tilde{I}p_t, r, \phi)$ is used for picking pixel values of the polar image around the location $\vartheta\{c_t(s)\}, R\{c_t(s)\}$. The pixel values can be weighted by a mask. $\tilde{I}p_t$ and $\tilde{I}p_{t+1}$ are the Gaussian smoothed ($\sigma = 1$ and support 5) Ip_t and Ip_{t+1}, respectively.

Additionally, intensity changes (due to patient movement or acquisition parameter adjustment) are also accounted

$$\tilde{I}p_{t+1} = (Ip_{t+1} - (\overline{Ip_{t+1}} - \overline{Ip_t})) * h_{gauss},$$

where $\overline{Ip_{t+1}}$ and $\overline{Ip_t}$ are the intensity averages of the myocardium area in all polar images.

Due to the low resolution of cine MRI and BOLD imaging and the relative low contrast, the contour detection of the previous section might include contour points that are not the true LV boundary. To compensate for such small errors, a 1×7 area along the radius is scanned and the minimum is chosen as shown on the last term of Eq.(1). In some cases, a contour correction may not always be desirable since (i) errors in the previous contour will propagate and (ii) erroneous image contours (on strong edges) might get selected.

Finally, the total energy is defined as:

$$E_{tot} = \sum_{s=1}^{L_t} \sum_{k=1}^{L_{t+1}} M_t(s,k) \cdot E(c_t(s), c_{t+1}(k)) \, .$$

3.2. DP Implementation

The following propagation equation is solved with DP as in [12]

$$E_{tot}(s,k) = \min_{p=1\ldots L_{t+1}} \{E_{tot}(s-1,p) + E(c_t(s), c_{t+1}(k))\} \, ,$$

where $E_{tot}(s-1,p)$ denotes the minimum cumulative cost for traversing at point $M_t(s-1,p)$ in the matching unit. The computation starts at $M_t(1,1)$ and is repeated until the cumulative cost is calculated for traversing at point $M_t(L_t, L_{t+1})$. The minimum at $c_t(L_t)$ is backtracked to derive the global solution.

4. EXPERIMENTAL RESULTS

Cardiac cine MR images were obtained from a healthy volunteer using a Siemens Sonata (1.5T) scanner, and were breath-held and ECG-gated. Following scout scans, a single short-axis slice of the left ventricle (LV) were acquired in the cine mode with 2-D balanced SSFP technique. Scan parameters: voxel size $= 0.9 \times 0.9 \times 6 \; mm$; flip angle $= 45^o$; $TR/TE = 3.1/1.5 \; ms$; 20 cardiac phases.

The algorithms were implemented in MATLAB. The DICOM images ($N = 20$) were imported into MATLAB and the end systolic frame (frame 10) and a center point were selected as reference. Starting from frame 10, the algorithms were executed once forward and backward to obtain results on the complete cine stack. In Fig.1, the epicardial and endocardial boundaries, and the corresponding six myocardial segments, are shown for two frames: the end systolic (frame 10) and the mid diastole. In Fig.2 the contours of frame 10 are shown in polar coordinates. Finally, in Fig.3, we show the epicardial LV contour of the end systolic and end diastolic frame, and the correspondence between the six segment points as propagated throughout the complete stack (set) of cine images.

Notice how tightly and accurately the contours are detected, especially in the regions with various edge profiles, and the papillary muscles are excluded successfully. The same consistency has been observed with other sequences as well. Extensive synthetic experiments and experiments on other sequences have been performed to define normalization and weight factors factors; however, their presentation is beyond the space allotted in this article.

5. CONCLUSION

An automated method to detect the epicardial and endocardial contours of the LV in short axis cardiac cine MR images in the polar coordinate system was presented. In addition consecutive epicardial contours are elastically matched to the contour of the end systolic (reference) frame. A DP approach was chosen. In its present form,

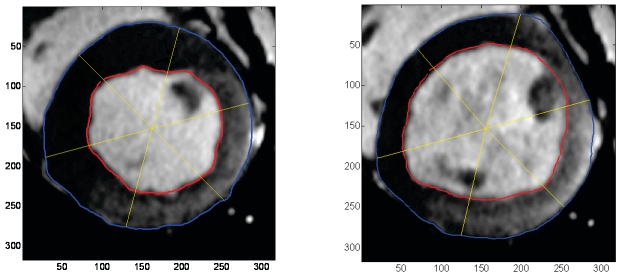

Fig. 1. Two frames in Cartesian coordinates with their corresponding endocardia, epicardial, and six segment points marked.

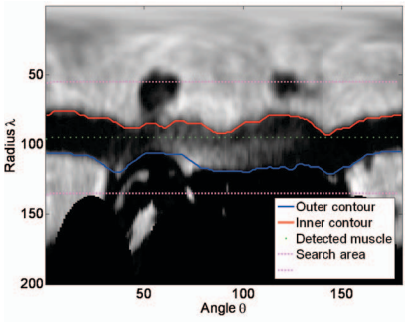

Fig. 2. An MR image in systole transformed into polar coordinates.

the algorithm requires minimal parameter corrections among different MRI sequences. In the future the algorithm will be compared with hand labeled contours from imaging experts. Furthermore, the majority of user initialization could be eliminated by employing an LV detection algorithm as in [5]. Successful implementation of the method would provide a systematic and robust method for evaluating cardiac phase-resolved myocardial MRI signal changes.

6. REFERENCES

[1] O. Pereztol-Valdes, J. Candell-Riera, C. Santana-Boado, J. Angel, S. Aguade-Bruix, J. Castell-Conesa, E. V. Garcia, and J. Soler-Soler, "Correspondence between left ventricular 17 myocardial segments and coronary arteries," *Eur Heart J*, vol. 26, no. 24, pp. 2637–2643, December 2005.

[2] R. Dharmakumar, J. M. Arumana, A. C. Larson, Y. Chung, G. A. Wright, and D. Li, "Cardiac phase-resolved blood oxygen-sensitive steady-state free precession MRI for evaluating the functional significance of coronary artery stenosis," *Invest Radiol*, vol. 42, no. 3, pp. 180–188, Mar 2007.

[3] P. Kellman, A.C. Larson, L.-Y. Hsu, Y.-C. Chung, O.P. Simonetti, E.R. Mcveigh, and A.E. Arai, "Motion-corrected free-breathing delayed enhancement imaging of myocardial infarction," *Magn. Reson. in Med.*, vol. 53, no. 1, pp. 194–200, 2005.

[4] C. Dornier, M. K. Ivancevic, P. Thévenaz, and J. P. Vallée, "Improvement in the quantification of myocardial perfusion using an automatic spline-based registration algorithm," *J. Magn. Reson. Imaging*, vol. 18, no. 2, pp. 160–168, August 2003.

[5] A. Pednekar, U. Kurkure, R. Muthupillai, S. Flamm, and I. A. Kakadiaris, "Automated left ventricular segmentation in cardiac MRI," *IEEE Trans. Biomed. Eng.*, vol. 53, no. 7, pp. 1425–1428, 2006.

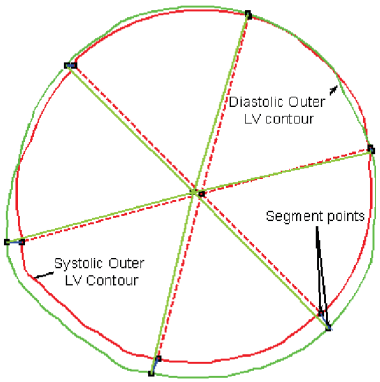

Fig. 3. Elastic matching between two images.

[6] C. Pluempitiwiriyawej, J. M. F. Moura, Yi-Jen L. Wu, and C. Ho, "STACS: new active contour scheme for cardiac MR image segmentation," *IEEE Trans. Med. Imag.*, vol. 24, no. 5, pp. 593–603, 2005.

[7] A. F. Frangi, W. J. Niessen, and M. A. Viergever, "Three-dimensional modeling for functional analysis of cardiac images, a review," *IEEE Trans. Med. Imag.*, vol. 20, no. 1, pp. 2–5, 2001.

[8] M. Sermesant, P. Moireau, O. Camara, J. Sainte-Marie, R. Andriantsimiavona, R. Cimrman, D. L. G. Hill, D. Chapelle, and R. Razavi, "Cardiac function estimation from MRI using a heart model and data assimilation: Advances and difficulties," *Functional Im. and Modeling of the Heart*, pp. 325–337, 2005.

[9] S. C. Mitchell, J. G. Bosch, B. P. F. Lelieveldt, R. J. van der Geest, J. H. C. Reiber, and M. Sonka, "3-d active appearance models: segmentation of cardiac mr and ultrasound images," *IEEE Trans. Med. Imag.*, vol. 21, no. 9, pp. 1167–1178, 2002.

[10] N. Paragios, "A variational approach for the segmentation of the left ventricle in mr cardiac images," in *Proc. IEEE Workshop Variational and Level Set Meth. in Comp. V. 2001*, 2001, pp. 153–160.

[11] M.-P. Jolly, "Combining edge, region, and shape information to segment the left ventricle in cardiac MR images," in *Proceedings of MICCAI 2001*, London, UK, 2001, pp. 482–490.

[12] D. Geiger, A. Gupta, L. A. Costa, and J. Vlontzos, "Dynamic programming for detecting, tracking, and matching deformable contours," *IEEE Trans. PAMI*, vol. 17, no. 3, pp. 294–302, 1995.

[13] B.C.S. Tom, S.N. Efstratiadis, and A.K. Katsaggelos, "Motion estimation of skeletonized angiographic images using elastic registration," *IEEE Trans. Med. Imag.*, vol. 13, no. 3, pp. 450–460, Sep 1994.

[14] Y. Chen, T. S. Huang, and Y. Rui, "Optimal radial contour tracking by dynamic programming," in *ICIP 2001*, 2001, vol. 1, pp. 626–629.

[15] Z. Wang, R.K. Raghunath, and J. Ben-Arie, "Optimal ramp edge detection using expansion matching," *IEEE Trans. PAMI*, vol. 18, no. 11, pp. 1092–1097, 1996.